

Multiple H-Bonding Chain Extender-Based Ultrastiff Thermoplastic Polyurethanes with Autonomous Self-Healability, Solvent-Free Adhesiveness, and AIE Fluorescence

Yuan Yao, Ziyang Xu, Bo Liu, Meng Xiao, Jianhai Yang,* and Wenguang Liu*

Developing an autonomous room temperature self-healing supramolecular polyurethane (PU) with toughness and stiffness remains a great challenge. Herein, a novel concept that utilizes a T-shaped chain extender with double amide hydrogen bonds in a side chain to extend PU prepolymers to construct highly stiff and tough supramolecular PU with integrated functions is reported. Mobile side-chain H-bonds afford a large flexibility to modulate the stiffness of the PUs ranging from highly stiff and tough elastomer (105.87 MPa Young's modulus, 27 kJ m⁻² tearing energy), to solvent-free hot-melt adhesive, and coating. The dynamic side-chain multiple H-bonds afford an autonomous self-healability at room temperature (25 °C). Due to the rapid reconstruction of hydrogen bonds, this PU adhesive demonstrates a high adhesion strength, fast curing, reusability, long-term adhesion, and excellent low-temperature resistance. Intriguingly, the PU emits intrinsic blue fluorescence presumably owing to the aggregation-induced emission of tertiary amine domains induced by side-chain H-bonds. The PU is explored as a counterfeit ink coated on the predesigned pattern, which is visible-light invisible and UV-light visible. This work represents a universal and facile approach to fabricate supertough supramolecular PU with tailorable functions by chain extension of PU prepolymers with multiple H-bonding chain extenders.

1. Introduction

Polyurethanes (PUs) are a versatile group of polymers with widely ranging structures and properties because they can be synthesized from a step-growth polymerization between diverse polyisocyanates and polyols, and tuned by selecting suitable chain extenders and end-groups.^[1] PUs find widespread applications as elastomers, fibers, foams, adhesives/varnish, sealants, and so on.^[2] Recently, self-healing PUs have attracted considerable attention due to their recyclability and huge implications for the

reduction of environmental burden. Among these, supramolecular PUs constructed from reversible non-covalent interactions such as hydrogen bond,^[3] host–guest interaction,^[4] metal–ligand coordination,^[5] ionic interaction,^[6] π – π stacking^[7] and (aromatic) disulfide bond,^[8] demonstrate intrinsic self-healability and reprocessability. In particular, the H-bonds whose bond strengths depend on the nature of donor and acceptor are the most commonly employed to construct self-healing PUs because of their directionality, responsiveness, and stability.^[9] Although there are abundant H-bond motifs in the backbone, this single hydrogen bond is generally not strong enough for stiffening and toughening PU materials after healing.^[10] And it is commonly accepted that there is an inherent paradox between mechanical stiffness and self-healing ability: strong bonds result in increased stiffness but less efficient healing, while weak bonds afford efficient healing, but yield relatively soft materials.^[11]

To address this paradox, Guan et al. designed a hard–soft multiphase-separated structure by self-assembly of hydrogen-bonding brush polymers. The soft segment carrying H-bonds afforded self-healing capacity, and the hard segment served to stiffen the network, thus concurrently achieving the enhanced stiffness and self-healability.^[12] In the follow-up study, they also developed the diblock copolymers end-functionalized with a quadruple H-bonding motif of 2-ureido-4-pyrimidinone (UPy), which exhibited high rigidity (Young's modulus of 21.1 MPa), but the self-healing behavior was needed to be triggered by temperature (45 °C).^[13] Thus far, several design strategies have been developed to construct multiphase-separated healable supramolecular PU with tunable soft segments and hard segments by combining the weak H-bonds in the urethane with other non-covalent interactions in main chain.^[14] Nevertheless, these approaches are mainly based on the non-covalent interactions in the main chains and the special designs of either soft segment or hard segment. Besides, due to the constrained mobility of backbone, input of external energy (either heat or light)^[15] or addition of metal ions^[16] is required to achieve self-healing. These complex preparation and external stimulus/intervention

Y. Yao, Z. Xu, B. Liu, M. Xiao, Prof. J. Yang, Prof. W. Liu
School of Materials Science and Engineering
Tianjin Key Laboratory of Composite and Functional Materials
Tianjin University
Tianjin 300350, China
E-mail: jianhaiyang@tju.edu.cn; wgliu@tju.edu.cn

 The ORCID identification number(s) for the author(s) of this article can be found under <https://doi.org/10.1002/adfm.202006944>.

DOI: 10.1002/adfm.202006944

may limit their application scope. To the best of our knowledge, it is rarely reported that thermoplastic PUs were prepared by combining the main chain H-bonds with the non-covalent interactions in the side chain with a high mobility. Lately, Li et al. reported a supertough healable PU tethering ultra-strong H-bonds of UPy in the side chains. Nevertheless, 1,4-butanediol were heated to 100 °C for achieving 90% healing efficiency of tensile strength within 24 h.^[15a] Therefore, developing a facile and simplified universal approach to fabricate supramolecular PU with high toughness/stiffness and autonomic room temperature self-healing still remains a major challenge.

Recently, we developed a series of high-strength self-healable supramolecular poly(*N*-acryloyl glycinamide) (NAGA) and copolymer hydrogels based on dual amide hydrogen bonds in the side chain.^[17] We discovered that the mobile side-chain H-bonds afforded a large flexibility to modulate the stiffness of the hydrogels ranging from highly stiff bioscaffolds to soft injectable hydrogels. This reminds us of constructing supramolecular PUs by side-chain hydrogen-bonding reinforcement. It is known that a chain extender is used extensively to manufacture PU cast elastomers, offering a large freedom to tailor the mechanical properties.^[18] However, no literature has reported on preparation of highly stiff PUs with an autonomic room temperature healability solely by strengthening of chain extender. Taking into account the advantage of side-chain hydrogen bonds and flexibility of chain extender in regulating mechanical properties, we proposed, for the first time, a new notion of

multiple H-bonding chain extender strengthening mechanism to prepare ultrastiff and repairable supramolecular PUs. We designed and synthesized a novel side-chain hydrogen-bonding chain extender starting from NAGA monomer. The synthetic route is depicted in Figure S1a, Supporting Information, where NAGA is reacted with diethanolamine (DEA) to form a T-shaped chain extender diol (named as OH–NAGA–OH), whose main chain is terminated with two hydroxyls, and side chain is consisted of dual amide multiple H-bonds. We used it to construct supramolecular PUs by chain extending reaction (Figure 1a), and hypothesized that combining the backbone H-bonds with side-chain H-bond would contribute to a multiphase-separated supramolecular PU with customizable mechanical stiffness and self-healing ability (Figure 1b). This novel OH–NAGA–OH chain extender would endow the supramolecular PU elastomer with a high stiffness and tear resistance as well as fast autonomous self-healing ability at room temperature. Remarkably, by adjusting the content of the chain extender, we could develop a solvent-free PU hot-melt adhesive in that OH–NAGA–OH could be melted at a high temperature and reacted with PU prepolymer to form a flexible PU film, which could be softened at an elevated temperature to strongly adhere to diverse materials upon cooling and even at a low temperature. The adhesive could be used repeatedly if it was subjected to cyclic heating and cooling. Intriguingly, the aggregation-induced emission (AIE) property resulted from the specific tertiary amine structure of OH–NAGA–OH could allow for development of a fluorescent PU coating toward anti-counterfeiting applications.

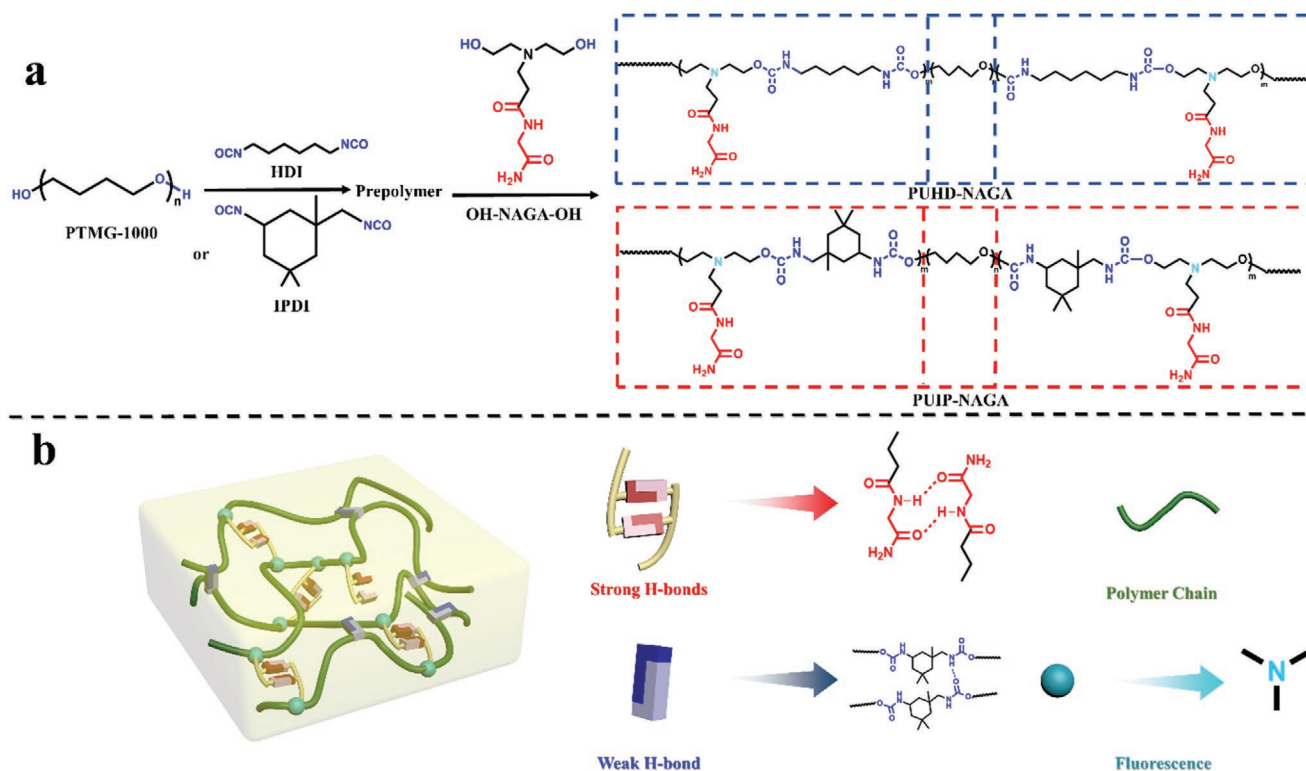


Figure 1. Synthesis of supramolecular PU elastomer via reaction of multiple hydrogen-bonding chain extender with prepolymer. a) Synthesis and chemical structures of PUHD-NAGA and PUIP-NAGA PU elastomers. b) Schematic illustration of hydrogen-bonding reinforcement in PU network.

2. Results and Discussions

2.1. Preparation and Characterization of Polyurethanes

To verify our concept, we first synthesized a novel T-shaped chain extender OH–NAGA–OH carrying double amide group in side chain by the Michael addition reaction between NAGA with DEA. The chemical structure of OH–NAGA–OH was confirmed by ^1H NMR spectra (Figure S2b, Supporting Information). The desired supramolecular PUs carrying double amide groups in the side chain were obtained by two-step reactions, that is, preparation of PU prepolymer by the reaction of isophorone diisocyanate (IPDI, or hexamethylene diisocyanate [HDI]) with polytetramethylene ether glycol (PTMG), followed by chain extension reaction of PU prepolymer with OH–NAGA–OH (Figure 1). The final PU was named as PUIP-NAGAx (or PUHD-NAGAx), where x denotes the molar ratio of OH–NAGA–OH to PTMG. As shown in the FTIR spectra (Figure S3, Supporting Information), the absorption bands at 3300 and 1540 cm^{-1} are attributed to the stretching and bending vibration of N–H. The stretching vibration region of C=O groups is split into two peaks at 1693 and 1647 cm^{-1} , which are ascribed to free C=O groups and hydrogen-bonded C=O groups, respectively.^[14c,15b] The characteristic peak of –NCO does not appear at 2260–2280 cm^{-1} in the spectra, proving that –NCO of IPDI completely reacted with –OH to form urethane. The ^1H NMR result also confirms the structures of the prepolymer (PUIP) and as-prepared PU (PUIP-NAGA) (Figure S4, Supporting Information). The PUIP-NAGA films could be dissolved in various organic solvents including methanol, ethanol, dimethyl sulfoxide, chloroform, and also could be remolded into new films (Figure S5, Supporting Information), hinting that the PUIP-NAGA could be recycled by a simple dissolving and reprocessing method. The molecular weights and distributions of PUIP-NAGA are shown in Table S1, Supporting Information. All these results indicate the successful synthesis of PUIP-NAGA PUs, and they were cross-linked by supramolecular dynamic H-bonds.

To highlight the strengthening effect of dual amide multiple hydrogen bonds of NAGA diol, we also synthesized the other T-shaped chain extender OH–AAM–OH carrying a single amide group to make a parallel comparison (Figures S1b and S2a, Supporting Information). PTMG with a linear structure served as a soft segment, and different diisocyanates and chain extenders were utilized to adjust the mechanical properties. The prepolymers were obtained via reaction of PTMG with IPDI (containing an asymmetric alicyclic structure) or reaction of PTMG with HDI (containing saturated aliphatic structure). Then, the PU prepolymer was separately reacted with the chain extender carrying a single amide (OH–AAM–OH) or dual amide (OH–NAGA–OH) or butyl side chain (*N*-butyldiethanolamine, BIDE) to form PUs with different hard segment domains. The PUIP polymer without chain extending reaction exhibits weak mechanical properties with a tensile strength of 60 kPa and an elongation at break of 760% (Figure S6, Supporting Information). Once adding chain extender BIDE, the obtained PU (PUIP-BIDE) is too viscous to form a film since there are no H-bonding interactions in the side chain of BIDE (Figure S7, Supporting Information); while a better film

forming ability is observed for the PUs obtained from both OH–NAGA–OH and OH–AAM–OH chain extending reactions. It is seen that the mechanical properties of the PUHD-AAM, PUHD-NAGA, PUIP-AAM, and PUIP-NAGA are enhanced due to hydrogen-bonding reinforcement (Figures S8 and S9, Supporting Information). The results indicate that the mechanical properties of the PUs can be modulated by varying diisocyanate species (stiff alicyclic IPDI, flexible aliphatic HDI) and the chain extender with/without H-bonds. Among all the obtained PUs, the PUIP-NAGA exhibits the highest mechanical properties due to combined hydrogen-bonding and alicyclic ring stiffening effect. So this PU will be selected for further evaluation of the thermal, mechanical, self-healing, and adhesive properties.

Next, the thermal stability of PUIP-NAGA PU was analyzed. The thermogravimetric analysis (TGA) curves of PUIP-NAGA show two distinct weight loss stages in the range of 240–350 $^{\circ}\text{C}$ and 350–440 $^{\circ}\text{C}$, respectively (Figure S10, Supporting Information). The first stage originates from the decomposition of the hard segment in the PUIP-NAGA network,^[19] and the second stage is attributed to the decomposition of the soft segments, suggesting a better thermal stability of PUIP-NAGA. XRD characterization shows no crystalline peak in the PUIP-NAGA (Figure S11, Supporting Information). A melting endothermic peak of crystalline PU is not observed either in the differential scanning calorimetry (DSC) curves over a temperature range from –80 to 180 $^{\circ}\text{C}$ (Figure S12, Supporting Information), suggesting the amorphous nature of the PUIP-NAGA. As presented in the figure, the glass transition temperatures (T_g) of the PUIP-NAGA are below 25 $^{\circ}\text{C}$. These outcomes hint that additional side-chain hydrogen bonds, amorphous structure, and low T_g would endow the PUIP-NAGA with high-strength, thermoplasticity, and room temperature (25 $^{\circ}\text{C}$) self-healing ability.

2.2. Mechanical Properties of PUIP-NAGA

In our experiment, we noticed that the PUIP-NAGA films were able to withstand various deformations, including bending, twisting, and curling (Figure S13, Supporting Information). The mechanical properties of PUIP-NAGA films with varied molar ratios of OH–NAGA–OH/PTMG were evaluated by tensile test. In the tensile stress–strain curves, an initial stiffening region, and a subsequent steady region emerge until occurrence of rupture due to the presence of inter-chain dynamic H-bonds in the PUIP-NAGA network (Figure 2a). A similar phenomenon has been reported in the previous literature.^[14b] The PUIP-NAGA1.6 can be stretched to over 22 times (2200%) its original length without rupture at a loading rate of 50 mm min^{-1} , and the tensile strength and Young's modulus are 10 kPa, and 1.31 MPa, respectively. With increasing the OH–NAGA–OH content, the number of hard segments is accordingly increased, which act as H-bonding cross-linkages. Combining side-chain dual amide multiple hydrogen-bonding interactions and hard segmental cross-links contributes to a tremendous increase in the mechanical strength and Young's modulus. It is shown that the tensile strength, Young's modulus, and elongation at break of PUIP-NAGA2.1 are 1.89 MPa, 28.18 MPa, and 780%,

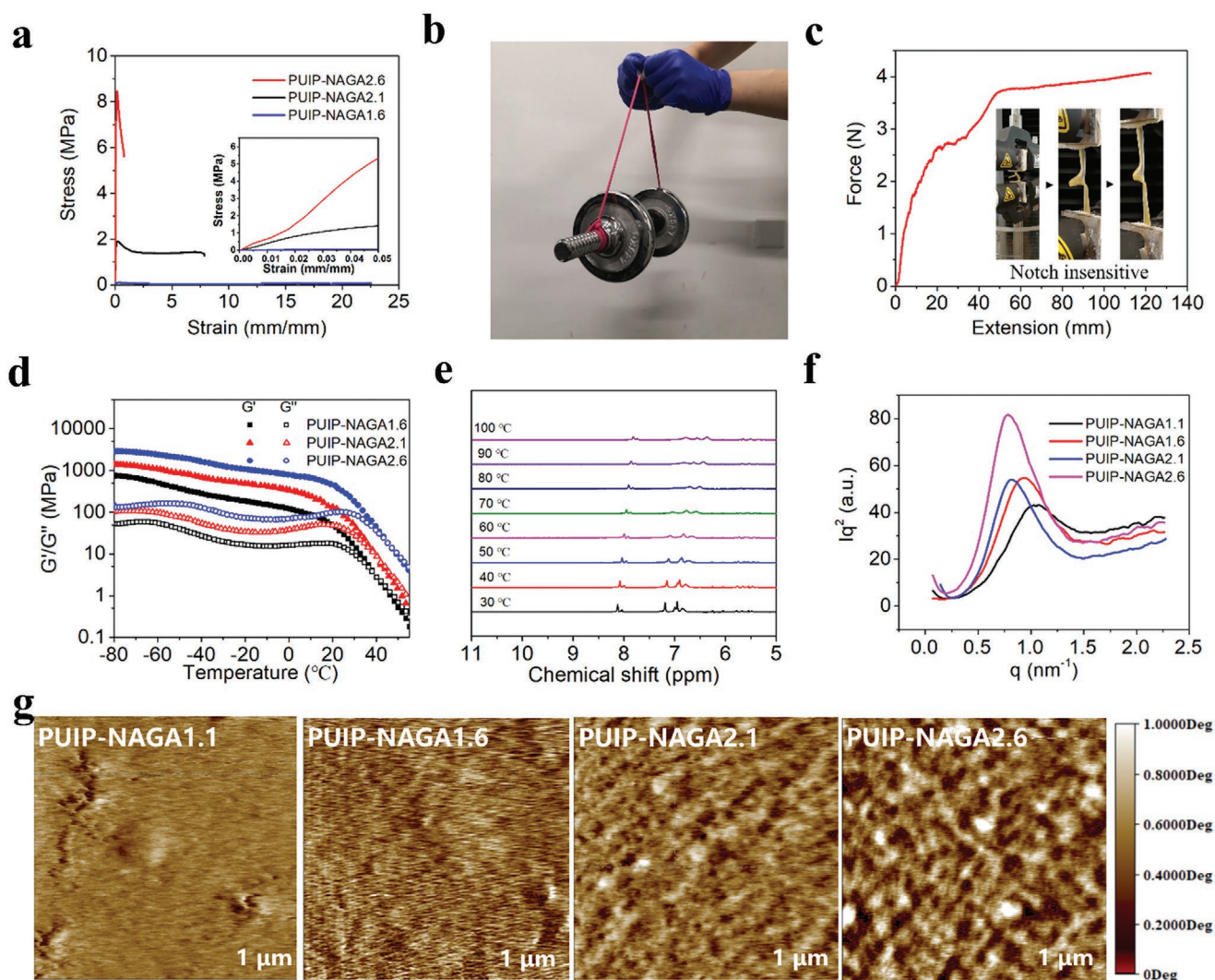


Figure 2. Characterization of the basic mechanical properties and multiphase morphology of the PUIP-NAGA. a) Typical strain–stress curves of the PUIP-NAGA elastomer. Inset is partial enlarged drawing of small strain. b) Photograph showing that the PUIP-NAGA2.6 film could withstand a 4 kg dumbbell. c) Trouser tearing curve of PUIP-NAGA2.6 film and process of its notch passivation. d) Variations in the storage moduli of PUIP-NAGA as a function of temperature. e) VT-1H NMR spectra of the PUIP-NAGA2.1 recorded under different temperatures. f) Iq^2 – q profiles of the PUIP-NAGA. g) AFM images of PUIP-NAGA films.

respectively, while the PUIP-NAGA2.6 demonstrates 8.46 MPa tensile strength, 105.87 MPa Young’s modulus, and 78% elongation at break. In comparison, the modulus value of PUIP-NAGA2.1 and PUIP-NAGA2.6 is respectively increased to over 20–80 times as that of PUIP-NAGA1.6. While the elongation at break is significantly decreased due to the high density of hydrogen-bonding cross-links.

Figure S14, Supporting Information shows a pronounced hysteresis in the loading–unloading curves even in the low-strain region (50%), implying the occurrence of energy dissipation during the rupture of the hydrogen bonds in the stretching process. When the specimen was extended to a 200% strain, a larger hysteresis area with dissipation energy of 2.52 MJ m^{-3} is observed after the first loading–unloading cycle.

More interestingly, a PUIP-NAGA2.6 film with a width of 10 mm and thickness of 2.5 mm can lift a weight of 4 kg with only a little deformation, which is impossible for traditional soft

rubber to withstand (Figure 2b). The tear resistance of PUIP-NAGA2.6 was further evaluated by stretching a trouser specimen to break. As shown in Figure 2c and Movie S1, Supporting Information, the notch-insensitive PUIP-NAGA2.6 could resist tearing, and the notch becomes significantly blunt during the stretching process. The tearing energy of PUIP-NAGA2.6 is estimated as 27 kJ m^{-2} , exhibiting a high tear resistance ability. Such outstanding properties are attributed to the synergistic effect of combined weak backbone H-bonding^[20] and strong side-chain dual amide hydrogen-bonding interactions in the PUIP-NAGA network (Figure 1b). When stretched, the supramolecular PUIP-NAGA network can effectively dissipate strain energy through the rupture of weak H-bonds, whereas the strong H-bonds serve to stiffen the network.

To prove this, we proceed to prepare PUIP-AAm PUs carrying single amide groups on the side chains, which only could form weak single H-bonds and thus did not possess

multi-strength H-bonds.^[17a] The PUIP-AAm2.1 film can be stretched to 2395% but only exhibits a Young's modulus of 0.31 MPa. Even if the OH-AAm-OH content is significantly increased, the PUIP-AAm3.1 only presents a Young's modulus of 1.93 MPa, which is not a significant increment. The PUIP-AAm films are only partially elastic at an initial 30% strain and essentially undergo a continuous plastic deformation upon continuing to apply a tensile stress (Figure S9, Supporting Information). These results reveal that the cross-link strength of H-bonds in dual and single amide motifs are starkly different because much stronger hydrogen-bonding interactions are formed from the dual amide motifs than from the single amide motifs. Therefore, the dual amide multiple hydrogen bonds in the side chains of PU act as strong cross-linkages, thus affording a high stiffness elasticity.

To further illustrate the chain mobility and viscoelastic behaviors of PUIP-NAGA containing multi-strength H-bonds, the temperature dependence of storage modulus (G') and loss modulus (G'') were tested by dynamic mechanical analysis. In Figure 2d, the PUIP-NAGA2.6 possesses the highest storage modulus than the others because of the denser multi-strength hydrogen-bonding cross-links. At about $-50\text{ }^{\circ}\text{C}$, a downward trend of the moduli increases, indicative of the onset of soft segment motion. As the temperature is above $20\text{ }^{\circ}\text{C}$, the moduli of all PUIP-NAGA polymers drop sharply, implying that the strong H-bonds in the dual amide motifs begin to dissociate. When the temperature is elevated to $60\text{ }^{\circ}\text{C}$, the sample film is softened and cannot maintain its shape due to the dissociation of most intermolecular hydrogen bonds. The dissociation kinetics of the H-bonds in PUIP-NAGA2.1 at different temperatures was further studied by variable temperature (VT) ^1H NMR spectroscopy. The variation in the hydrogen proton chemical shift of NH in the side-chain dual amide motif is shown in Figure 2e. When the temperature is higher than $60\text{ }^{\circ}\text{C}$, the chemical shift of NH is significantly reduced, suggesting that the intermolecular hydrogen bonds are largely dissociated at an elevated temperature. It is theoretically accepted that the formation of H-bonds reduces the density of the electron cloud, and imparts a shielding effect, thus increasing the chemical shift.^[10] Therefore, the feature peak of hydrogen proton shifts to the high field and becomes wider owing to the disruption of H-bonds as the temperature increases.^[10] Previous reports revealed that multiple H-bonds exert an obvious effect on the mechanical property because their aggregations lead to the formation of multiphase separation structure.^[3a,14c,15a] Herein, the microphase separation of the PUIP-NAGA was studied by small-angle X-ray scattering (SAXS) and atomic force microscope (AFM). As shown in the 2D graph and Iq^2-q curve (Figure 2f; Figure S15, Supporting Information), the PUIP-NAGA is not crystallized and only exhibits a short-range ordered structure. With an increase of OH-NAGA-OH content, the primary scattering peak shifts toward a smaller q value, with micro-region size increasing from 11.8 to 20.6 nm (Figure S16, Supporting Information). Also, the full width at half maximum of the scattering peaks is gradually narrowed, indicating that the boundaries of microphase separation structure become clearer.^[21] The AFM images display that the PUIP-NAGA possesses a microphase separation structure resulted from the aggregation of the soft

segments (PTMG, dark areas) and hard segments (H-bonded aggregates, bright areas). The PUIP-NAGA2.6 with the highest hard segment content exhibits the most distinctive microphase separation (Figure 2g). It is noted that the microphase domain sizes calculated by analyzing traces of the AFM image match the SAXS data and there is a similar variation trend, that is, as the OH-NAGA-OH content increases, the microphase domain size becomes larger due to the increased hydrogen-bonding interactions. Therefore, increasing OH-NAGA-OH content promotes not only the formation of strong H-bonds, but also microphase separation, thus enhancing the mechanical property and resolving the paradox between mechanical strength and self-healing capability.

2.3. Self-Healability and Adhesion Properties of PU Hot-Melt Adhesive

Taking into account the flexibility of side-chain dual amide hydrogen bonds, we inspected the autonomous reparability of PUIP-NAGA. The PUIP-NAGA2.1 demonstrates an excellent scratch elimination ability. The artificial scratch made on the surface of PUIP-NAGA2.1 almost vanishes after 6 h at ambient condition (Figure 3a). To quantitatively evaluate self-healing ability, a PUIP-NAGA2.1 strip was cut into two separate pieces with a scalpel, and brought into contact and healed at room temperature for different time periods. The healed specimen was tested under stretching with a strain rate of 50 mm min^{-1} (Figure 3b). Figure 3c shows that within the healing time frame, the healed PUIP-NAGA demonstrates a similar stress-strain curve as the original one. After healed for 15 min, the modulus of the PUIP-NAGA2.1 film is recovered to 2.96 MPa and the self-healing efficiency is 10.5%. The film healed for 1 h can be stretched to over 300%, and achieves a modulus of 10.3 MPa with a healing efficiency of 36.5%. The healing efficiency increases with healing time and reaches as high as 87.6% at 6 h. In this case, the force curve of the healed PUIP-NAGA2.1 film is nearly overlapped with that of the original sample, suggesting the efficient recovery of all the mechanical properties. In a sharp contrast, the healing efficiency of PUIP-NAGA2.6 film after 6 h is only 10.84% (Figure S17, Supporting Information). From the perspective of the molecular structure, the PUIP-NAGA2.6 possesses denser hydrogen-bonding cross-linked network, which restrains the mobility of polymer chains. Whereas the PUIP-NAGA2.1 molecular chains have a high mobility at room temperature due to its lower hydrogen-bonding interactions. A freely mobile polymer chain can facilitate the healing efficiency.

To further understand the stress relaxation caused by the dynamic network, the rheological frequency sweep curve of PUIP-NAGA2.1 at room temperature was measured. During the scanning process, G' and G'' show an intersection point, indicating that the polymer network evolves from a cross-linked and elastic state to a reversible and dynamic state (Figure 3d). The relaxation time (the inverse of the frequency at the cross-over point) of PUIP-NAGA2.1 is 390 s, which implies that the PUIP-NAGA has a rapid molecular reconstruction ability to enable an efficient and robust healing at room temperature. Compared with other self-healing PUs reported to date,^[3a,5b]

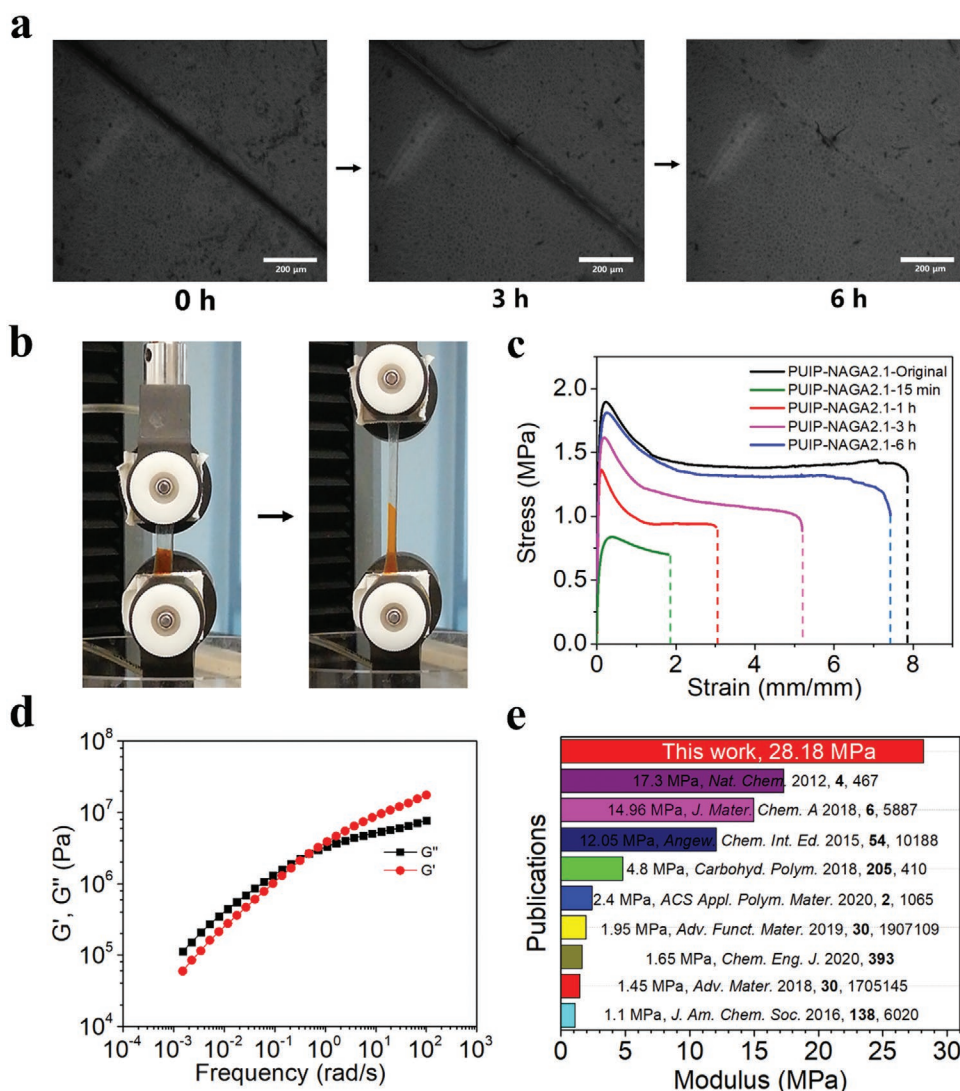


Figure 3. Self-healing properties of the PUIP-NAGA2.1 film. a) Optical microscopy images of artificially scratched PUIP-NAGA2.1 film and healing process. b) Digital images of the healed film before and after stretching. c) Stress–strain curves of a PUIP-NAGA2.1 film healed at room temperature for different times. d) Variation in storage shear modulus (G') and loss shear modulus (G'') of the PUIP-NAGA2.1 as a function of angular frequencies (ω) at room temperature. e) Comparison in modulus of the PUIP-NAGA2.1 with PU reported in literature.

our PUIP-NAGA has not only a record-high Young's modulus but also a shorter self-healing time (Figure 3e; Table S2, Supporting Information).

It is noted that the OH–NAGA–OH could be melted above 80 °C; thus it was mixed with the PTMG-IPDI prepolymer to directly form PUIP-NAGA polymer under a solvent-free condition. The temperature sweep curve of PUIP-NAGA shows that G' is always lower than G'' above 80 °C, indicating the PUIP-NAGA exhibits a liquid-like behavior at a high temperature (Figure 4a). The reason is that dynamic H-bonds are dissociated at a high temperature to afford a thermoplastic property. The dynamic H-bonds and thermoplasticity reminds us to explore the PUIP-NAGA as a hot-melt adhesive. In consideration of enhancing adhesion force between the adhered substrate and the hot-melt adhesive,^[22] the PUIP-NAGA with a higher content of side-chain dual amide H-bonds was selected for quantitatively evaluating the adhesion strength in bonding different substrates

including fiberglass board epoxy resin, aluminum, stainless steel, and ceramics. We also made a comparison with representative industrial thermoplastic PU adhesives such as Lubrizol-5173, Lubrizol-5174, BASF-60A, and Bayer-5733. The PUIP-NAGA film was sandwiched between two pieces of substrates, which were clamped by a clip, and placed in an oven at 100 °C for 20 min to promote adhesion. Then the substrates were cooled down to room temperature. As shown in Figure 4b, the adhered aluminum and stainless steel sheets are able to lift a dumbbell with a weight of 5 and 4 kg in the form of stretching and peeling, respectively. Figure 4c shows the lap-shear adhesion curves of the PUIP-NAGA and representative commercial thermoplastic PU adhesives in gluing stainless steel. Clearly, the PUIP-NAGA demonstrates the higher adhesion strength than all other commercial PU adhesives in bonding fiberglass board, aluminum, stainless steel, and ceramics sheets, achieving 15.60, 11.43, 7.57, and 15.71 MPa, respectively. The adhesion strength of PUIP-NAGA

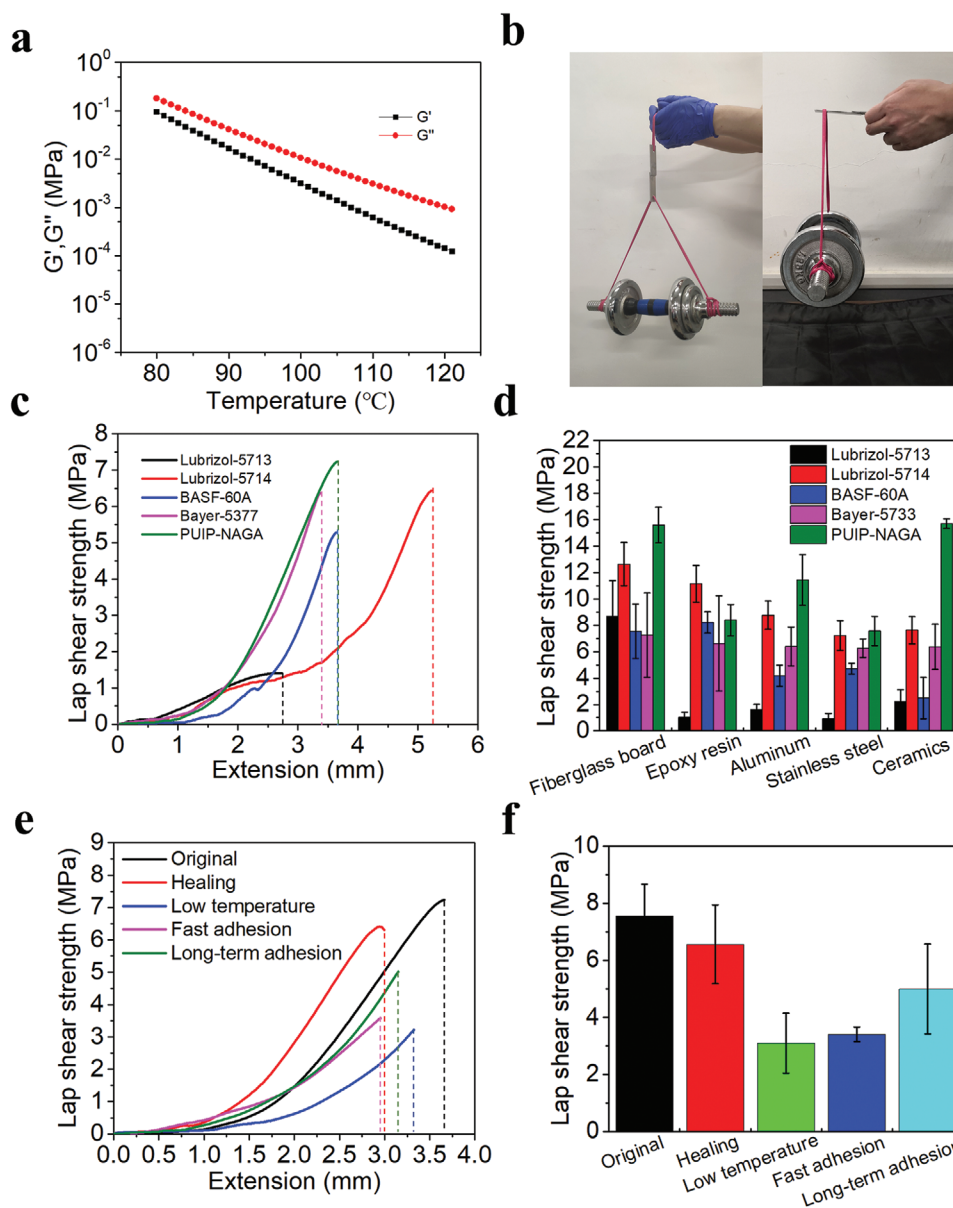


Figure 4. Adhesive properties of PUIP-NAGA. a) Storage shear modulus (G') and loss shear modulus (G'') of PUIP-NAGA at different temperatures. b) Digital images showing the ability of PUIP-NAGA bonded aluminum sheets and stainless steel sheets to lift a weight of 5 and 4 kg dumbbell, respectively. c) Lap-shear strength–extension curves of PUIP-NAGA and commercial adhesives in gluing stainless steel. d) Lap-shear strength of PUIP-NAGA and commercial adhesives in gluing different substrates. e) Lap strength–extension curves of PUIP-NAGA in gluing stainless steel under different conditions. f) Lap-shear strength of PUIP-NAGA in gluing stainless steel under different conditions.

in gluing the epoxy resin was 8.39 MPa, which is higher than that of Lubrizol-5173 (1.01 MPa) and Bayer-5733 (6.63 MPa), and comparable to that of Lubrizol-5174 (11.15 MPa) and BASF-60A (8.21 MPa) (Figure 4d). An explanation for its super adhesion capability is that at a melting state, more H-bonds in the PUIP-NAGA interact with the substrate surface and a higher cohesive strength is simultaneously achieved upon cooling. This collectively leads to a higher adhesion strength to diverse materials. We note that the hot-melt temperature of PUIP-NAGA is much lower than that of commercial thermoplastic PU adhesives (200 °C) due to the easier dissociation of dual amide H-bonds. In light of lower softening temperature, the PUIP-NAGA is advantageous over other

commercial PU adhesives in gluing easily deformable or melted materials at a high temperature such as polyvinylidene fluoride (PVDF) and polyethylene (PE). We can see that the PUIP-NAGA can robustly adhere to PE and PVDF with an adhesion strength of 0.83 MPa and 90 kPa, respectively. Of course, the adhesion strengths are relatively lower due to the low surface energy of PVDF and PE (Figure S18, Supporting Information). To the best of our knowledge, the adhesion strength of PUIP-NAGA is superior to that of the thermoplastic PU adhesives reported in the recent literature.^[23]

In addition, the PUIP-NAGA can still demonstrate a high adhesion strength even after shorter curing time. As shown

in Figure 4e,f, the initial adhesion strength of PUIP-NAGA in bonding stainless steel after 5 min curing at room temperature is 3.41 MPa, which is 45.1% of the ultimate adhesion strength. Owing to hydroxyl termination, the substrates adhered by PUIP-NAGA could be stored for a long time in an open environment, and achieved an adhesion strength of 5.0 MPa after 1-month storage. An adhesive is inevitably damaged during its service life, while an intrinsic self-healing ability can prolong its lifetime. Accordingly, we further evaluated the repeated adhesion strength of PUIP-NAGA in gluing stainless steel after self-healing. The PUIP-NAGA bonded stainless steel sheets were subjected to a lap-shear test until failure; the two separated sheets were reassembled and heated in an oven at 100 °C for 20 min, and cooled down to room temperature. The adhesion strength of healed PUIP-NAGA can still reach 6.57 MPa, which is comparable to that of the original adhesion strength (7.24 MPa). These results indicate that the strong adhesion, short curing time and self-healing of PUIP-NAGA originated from rapid dynamic exchange and reformation of H-bonds upon suffering to heating and cooling treatment.

Traditional thermoplastic PU adhesives are greatly affected by environmental factors especially in a high latitude and cold season, leading to adhesion failure and limiting their applications in harsh conditions. Next, we further examined the low-temperature resistance of the PUIP-NAGA adhesive. The bonded steel sheets were put in an ultra-low-temperature refrigerator (−80 °C) for 1 day. Then the bonded sheets were taken out, and the adhesion strength and working temperature of PUIP-NAGA were measured immediately. The adhesion strength of PUIP-NAGA is recorded as 3.1 MPa at −50 °C (Figure 4f), demonstrating a better low-temperature resistance. Overall, the PUIP-NAGA demonstrated a high initial and ultimate adhesion strength, fast curing, reusability, long storage time, and excellent low-temperature resistance, which make it a promising adhesive suited for applications in many fields such as electronics assembly, automotive, and aerospace industries.^[24]

2.4. AIE Fluorescence Property of PUIP-NAGA

One interesting phenomenon is that the PUIP-NAGA films can exhibit strong blue fluorescence under 365 nm UV light (Figure S19, Supporting Information). The PUIP-NAGA films demonstrate an absorption peak at 280 nm and an emission peak at 450 nm, whose intensity is increased with an increment of OH–NAGA–OH content (Figure 5a,b). Looking back at the molecular structure of the PUIP-NAGA, we find that it has tertiary amine moieties in the backbone and no aromatic structure exists. It has been identified that small molecules and polymers such as poly(amidoamine) dendrimer and poly(ethyleneimine) with tertiary amine structure emit strong blue fluorescence, which is non-traditional emission and closely related to $n-\pi^*$ interactions among the electron-rich groups.^[25] We also observed the blue luminescence of the OH–NAGA–OH solution, which was much stronger than that of OH–AAm–OH and BIDE because the formation of amidoamine structure by Michael addition reaction between DEA and NAGA could enrich $n-\pi^*$ transition and the strong H-bonds formed between the dual amide could facilitate this

process (Figure 5c; Figure S20, Supporting Information).^[26] Thus the tertiary amine structures in the PUIP-NAGA backbone may be the key cause of strong blue emission. Previous studies have shown that traditional chromophore-tethered fluorescent polymers cannot emit strong fluorescence in concentrated solutions or solid states due to the aggregation-induced quenching effect.^[27] However, many chromophore-free synthetic polymers and natural biopolymers are shown to emit unusual luminescence at the aggregation state, which is a well-known AIE.^[28] Thus, the PUIP-NAGA without any conventional chromophores exhibits strong blue emission at the solid-state, which is considered to result from AIE of tertiary amine. With an increment of the OH–NAGA–OH, the increased H-bond interactions induce the formation of aggregation domains of tertiary amines, thereby further enhancing fluorescence intensity in the solid state. The fluorescence color of PUIP-NAGA2.1 film exhibits a slight difference during stretching; while the fluorescence intensity of the stretched sample declines dramatically compared to the unstretched one (Figure 5d,e). The reason is that H-bond cross-links are broken under stretching, resulting in the disintegration of aggregation domains of tertiary amines. As a consequence, the weakening AIE effect causes the decrease of fluorescence intensity. To prove this AIE, the OH–NAGA–OH was dissolved into a 2 mol L^{−1} NaSCN solution, an H-bond breaking agent, and then its fluorescence intensity was recorded. As expected, the fluorescence intensity of OH–NAGA–OH remarkably decreased due to the breakup of H-bonds of dual amide motifs caused by NaSCN (Figure S21, Supporting Information). In addition, the PUIP-NAGA2.1 film was also immersed in a 2 mol L^{−1} NaSCN solution and its fluorescence intensity was measured. It is seen that the fluorescence intensity of the swollen film decreases dramatically due to the partial dissociation of the hydrogen bonds in NaSCN solution (Figure S22, Supporting Information). These results further confirm the phenomenon of AIE in our H-bonded PUs.

The PUs emitting photoluminescence (PL) have been reported previously; nevertheless, they were prepared by introduction of fluorescent organic dyes, fluorescent proteins, or quantum dots, etc.^[29] Few studies have reported on a multifunctional PU with strong intrinsic fluorescence in the solid-state. In addition, the PUIP-NAGA film exhibits over 95% transmittance over a visible wavelength range (400–800 nm) at room temperature, and the transparency remains almost unchanged with the variation of components (Figure 5f). This hints that microphase separation of soft segments and hard segments of PUIP-NAGA only leads to very small size of domains, which hardly influences light transmission. The unique intrinsic fluorescence property and high transparency can make PUIP-NAGA a promising anti-counterfeit ink. Invisible fluorescent anti-counterfeiting patterns are generally used in the field of anti-counterfeit printing, which can be seen under UV light but not identified by naked eyes. The PUIP-NAGA PU solution was cast on the surface of the poly(dimethylsiloxane) (PDMS) template patterned with the Tianjin University abbreviation, and the solvent was evaporated to obtain a transparent pattern (Figure 5g). The pattern cannot be observed under natural light. Once the pattern is exposed to an ultraviolet lamp, a fluorescent pattern is revealed clearly (Figure 5h). This visible-light invisible and UV-light visible PU holds appealing potential as anti-counterfeit ink or coating.

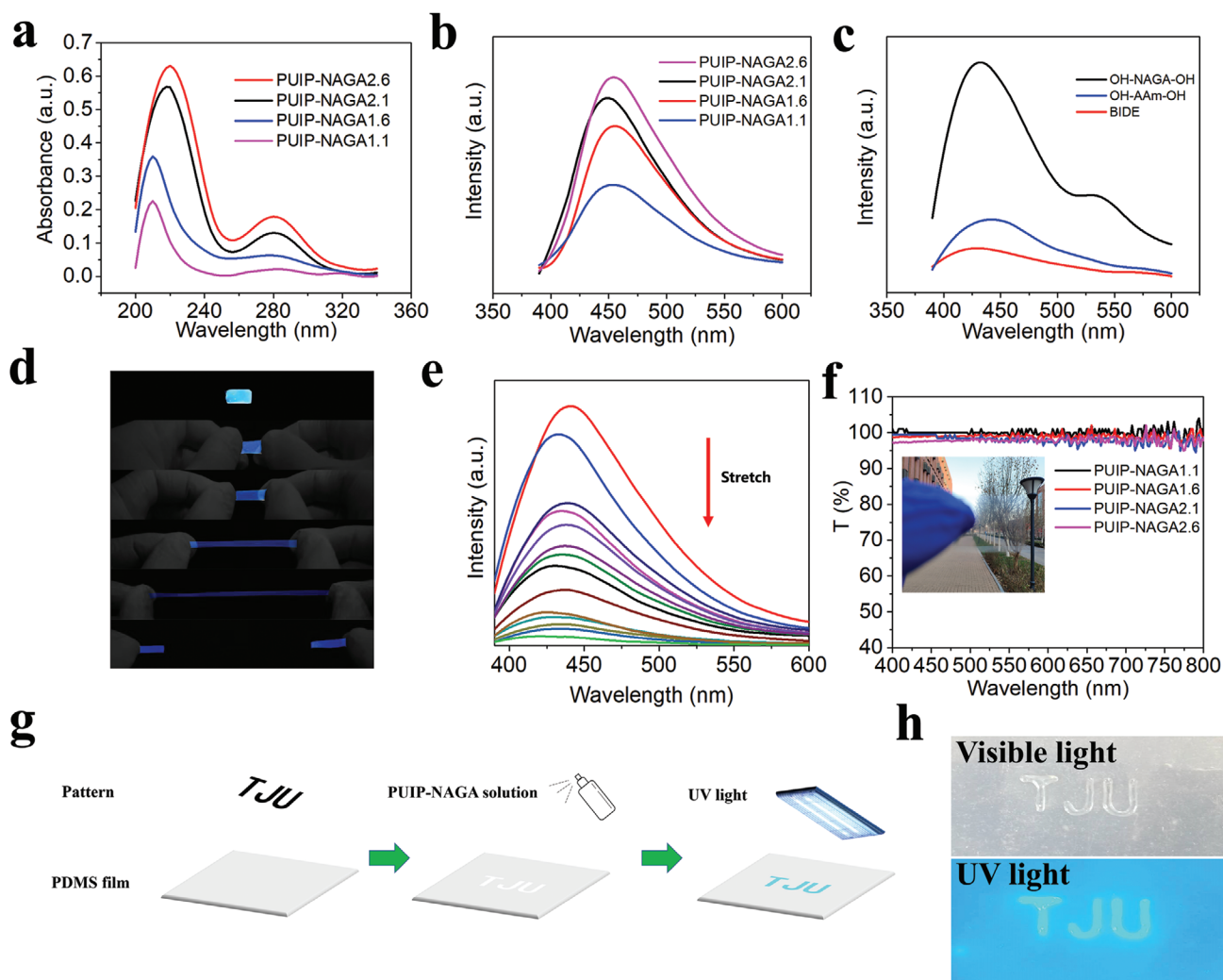


Figure 5. Fluorescence properties of the PUIP-NAGA films. a) UV-vis absorption spectra of PUIP-NAGA in methanol solution (0.1 mg mL^{-1}). b) Fluorescence spectra of PUIP-NAGA films. c) Fluorescence spectra of OH-NAGA-OH, OH-AAm-OH and BIDE. d) Fluorescence photos of PUIP-NAGA2.1 film before and after stretching excited by a 365 nm UV lamp. e) Fluorescence spectra of PUIP-NAGA2.1 film during stretching. f) Transmittance of PUIP-NAGA films to visible light ranging from 400 to 750 nm. Inset photograph is the PUIP-NAGA2.6 film. g) Anti-counterfeiting fluorescent pattern of PUIP-NAGA2.6 coating made on a PDMS film. h) Digital image of TJU pattern exposed to a 365 nm UV lamp.

3. Conclusions

In summary, we proposed to construct a highly stiff self-healable supramolecular PU based on a novel strengthening mechanism of multiple hydrogen-bonding chain extender (MHBCE) whose side chain carried two amides. We demonstrated that the reaction of MHBCE with PU prepolymer containing alicyclic or saturated aliphatic structure contributed to a highly stiff and tough supramolecular PU presumably due to combined reinforcement of side-chain and backbone hydrogen bonds. Mobile side-chain H-bonds afforded room temperature autonomous healability, allowing for flexible modulation PU properties ranging from highly stiff and tough elastomer to solvent-free hot-melt adhesive and coating. The solvent-free hot-melt PU adhesive was able to glue diverse materials with a high adhesion strength, short curing time, reusability, long storage time, and excellent low-temperature resistance. One interesting

phenomenon is that the PU could emit intrinsic blue intrinsic fluorescence supposedly owing to the AIE of tertiary amine domains induced by side-chain H-bonds. Benefiting from this unique feature, we explored this PU as a counterfeit coating with a predesigned pattern that is visible-light invisible and UV-light visible. This work points out a new design notion to fabricate supramolecular PU with customizable functions by chain extension of PU prepolymer with an MHBCE.

4. Experimental Section

Material: Glycinamide hydrochloride (98%), acryloyl chloride (98%), HDI (98%), and DEA (99%) were supplied from Tokyo Chemical Industry Co. Ltd (Shanghai, China). PTMG ($M_n = 1000 \text{ g mol}^{-1}$), IPDI (99%), dibutyltin dilaurate (97%, DBTDL), acrylamide (98%, AAm), and BIDE (98%) were purchased from Sigma-Aldrich (Shanghai, China). NAGA was synthesized according to the previous work.^[17a] All other

chemicals and solvents were analytical reagents and used as received without further purification.

Synthesis of *N, N*-bis(2-hydroxyethyl)-3-amino Propionyl Glycinamide: NAGA (10.0 g, 78 mmol) was dissolved in a mixed solvent of deionized water and methanol, followed by dropwise addition of 18 mL methanol solution of DEA (6.7 g, 64 mmol). The mixture was stirred at 40 °C for 24 h until the reaction was completed. Then the solvent was removed by rotary evaporation and the remaining solid was washed with acetone several times until neutral pH was achieved. The resultant product OH–NAGA–OH was dried in a vacuum oven. ¹H NMR (DMSO-d₆, 400 MHz): δ8.30 (t, 1H, CONHCH₂CONH₂), 7.29 (s, 1H, NH₂), 7.03 (s, 1H, NH₂), 4.41 (s, 2H, NCH₂CH₂OH), 3.61 (d, 2H, CONHCH₂CONH₂), 3.43 (t, 4H, NCH₂CH₂OH), 2.72 (t, 2H, NCH₂CH₂OH), 2.53 (t, 4H, NCH₂CH₂OH), and 2.27 (t, 2H, NCH₂CH₂CO) ppm.

Synthesis of *N, N*-bis(2-hydroxyethyl)-3-amino Propanamide: *N, N*-bis(2-hydroxyethyl)-3-amino propanamide (OH–AAM–OH) was synthesized according to the previously described method.^[30] An aqueous solution of DEA (6.7 g, 64 mmol) was added to the aqueous solution of AAM (4.6 g, 64 mmol). The reaction mixture was stirred at room temperature for 4 h, and then the solvent was evaporated by rotary evaporation to obtain a crude product as a pale yellow viscous liquid. ¹H NMR (DMSO-d₆, 400 MHz): δ7.33 (s, 1H, NH₂), 6.75 (s, 1H, NH₂), 4.34 (s, 2H, NCH₂CH₂OH), 3.41 (t, 4H, NCH₂CH₂OH), 2.69 (t, 2H, NCH₂CH₂CO), 2.51 (t, 4H, NCH₂CH₂OH), and 2.17 (t, 2H, NCH₂CH₂CO) ppm.

Preparation of Polyurethane: PTMG (1.5 g, 1.50 mmol) was heated at 120 °C in a 100 mL three-necked glass flask under vacuum and mechanically stirred for 2 h to remove water. An appropriate amount of IPDI (or HDI) and catalyst DBTDL (one drop) was added into the melted PTMG at 70 °C under a nitrogen atmosphere and further stirred for 3 h. The OH–NAGA–OH solution in dimethylacetamide (DMAc) was then added into the PU prepolymer to complete the reaction at room temperature for 18 h to obtain the final polymer. Other PUs were also prepared in the same way except for replacing the chain extender OH–NAGA–OH with OH–AAM–OH. The PU films were prepared by the solvent casting method on the customized Teflon plates and then dried at 70 °C for 48 h to remove DMAc under vacuum.

Preparation of PUIP-NAGA Hot-Melt Adhesive: PTMG (1.5 g, 1.5 mmol) was heated at 120 °C in a 100 mL three-necked glass flask under vacuum and mechanically stirred for 2 h to remove water. Then, IPDI (1.4 g, 6.15 mmol) and one drop of catalyst DBTDL were added into the melted PTMG at 70 °C under a nitrogen atmosphere and further stirred for 3 h. Subsequently, the OH–NAGA–OH (1.1 g, 4.65 mmol) was melted at 80 °C, and added into the above PU prepolymer. After a few minutes, the viscosity of the mixture rose significantly, and then the temperature was raised to 100 °C with continuous stirring for 18 h to obtain a solid product.

Preparation of Fluorescent Anti-Counterfeiting Pattern: A PDMS film with good optical transparency and non-fluorescence was chosen as a substrate material. The template of the pattern of Tianjin University abbreviation was attached on the surface of the PDMS film, and then a DMAc solution of PUIP-NAGA2.6 was sprayed evenly on the pattern template surface. Finally, the template was removed and the PUIP-NAGA coated-PDMS film was dried in vacuum to form a colorless and transparent pattern.

Characterizations: The ¹H NMR analysis was performed on a nuclear magnetic resonance (NMR) spectrometer (AVANCE III, 400 MHz, Bruker) using d-DMSO as the solvent. VT ¹H NMR spectra were recorded on a NMR spectrometer (ECZ600R, 600 MHz, JEOL) over a temperature range from 30 to 100 °C to detect the thermal dissociation of H-bonds. Gel permeation chromatography (1260 Infinity II, Agilent) was employed for evaluating molecular weight and molecular weight distribution. Polymethyl methacrylate standard was used for calibration. The chemical structures of PUIP-NAGA were characterized by a FTIR (Nicolet 6700, Thermo Scientific), operating in transmission mode from sample films cast onto KBr disks. The transparency of PUIP-NAGA films was determined by a UV–vis spectrophotometer (GENESYS 180UV, Thermo Scientific) with quick mode from 400 to 800 nm. The UV–vis absorption measurements of the PU solution in methanol were performed over a wavelength range from 200 to 340 nm. The crystal

phase of PUIP-NAGA was analyzed via XRD (D8 Advanced, Bruker) using Cu K α radiation ($\lambda = 0.154$ nm) from 5° to 50° at a scanning rate of 4 min⁻¹. The surface topographies of PUIP-NAGA films were observed on an AFM (CSPM5500A, Being Nano-Instruments) with the tapping mode. PL emission spectra were recorded on a fluorometer (FLS920, Edinburgh) at an excitation wavelength of 370 nm. Prior to fluorescence test, in order to ensure that the film thickness was consistent and uniform, the PUIP-NAGA solution with an identical concentration and volume was used, and the films were formed in the same customized Teflon mold plates.

Thermal Analysis: TGA was performed on a Simultaneous Thermal Analyzer instrument (STA449F3, Netzsch, Germany) with a heating rate of 20 °C min⁻¹ from 30 to 800 °C under nitrogen atmosphere. Before testing, samples were kept dry and weighed. DSC analysis was performed on a DSC instrument (200 F3, Netzsch, Germany) over a temperature range from –80 °C to 180 °C at a heating rate of 5 °C min⁻¹ under nitrogen atmosphere. The test process was heated twice to eliminate heat history and remove the influence of other factors.

Small-Angle X-Ray Scattering: The SAXS measurement was performed on a Bruker NanoSTAR system. A 10 mm × 5 mm × 1 mm film was fixed on the clear aperture of the sample stage, and then exposed to capture images. The X-ray wavelength was set at 0.154 nm, the distance between the sample and the detector was 1 050 mm, and the effective scattering vector range q ($q = 4\pi\sin\theta/\lambda$, where 2θ is the scattering angle and λ is the wavelength) was 0.2–2.2 nm⁻¹. 1D scattering intensity distribution was obtained by integrating the 2D scattering pattern, and the final result was analyzed.

Rheological Measurement: Rheological behaviors were recorded on a rheometer (MCR-302, Anton-Paar) with a 20 mm-diameter parallel steel plate. Frequency sweeps were performed at a strain amplitude of 0.1% in a frequency range from 0.001 to 100 rad s⁻¹ and temperature sweeps were performed at a frequency of 1 Hz in a temperature range from 80 to 100 °C. The disk sample with a diameter of 20 mm was pressed to the sandblasted parallel plate with a force of 5 N to avoid slippage.

Mechanical Testing: The PUIP-NAGA films were prepared by using a Teflon mold with a groove of 30 mm length × 8 mm width × 5 mm height. Mechanical tensile test was performed using a Legend 2344 electromechanical dynamometer (Instron, USA) at room temperature (25 °C) with a strain rate of 50 mm min⁻¹. Each measurement was repeated at least three times. The Young's modulus was calculated from the initial slope linear stage of the stress–strain curves. For tearing test, The PUIP-NAGA films were cut into trouser-shaped samples and tested in a tensile mode at a tensile rate of 50 mm min⁻¹. The tearing energy (Γ) could be calculated according to the following formula: $\Gamma = 2F/d$, where F is the average force at tearing, and d is the thickness of the trouser-shaped sample. Each measurement was repeated at least three times. The storage moduli and loss moduli of PUIP-NAGA films were measured on a Q800 Dynamic Mechanical Analyzer (TA, USA). The samples were pulled at a dynamic strain of 0.1% and a constant frequency of 1 Hz in a temperature range from –80 to 60 °C with a heating rate of 5 °C min⁻¹.

Fracture Self-Healing Test: To evaluate the self-healing ability of PUIP-NAGA films, the samples were stained respectively with methyl orange and methyl blue and cut into two pieces. The two pieces with different colors were brought into contact, but not overlapped, and then healed at different temperatures for different times. The healed samples were stretched following the above-mentioned procedure on a Legend 2344 electromechanical dynamometer to obtain the stress–strain curves. The mechanical self-healing efficiency was defined as the ratio of the restored Young's modulus to the original Young's modulus.

Lap-Shear Test: PUIP-NAGA and commercial PU adhesives were melted and reshaped into a film, then placed between two identical substrates and the overlapping area was measured. The two substrates were pressed gently and held by two paper clips and cured in an oven at 100 °C for 20 min and then cooled down to room temperature. The lap-shear testing was performed on a Legend 2344 electromechanical dynamometer at a strain rate of 50 mm min⁻¹ to obtain the lap-shear strength. Each measurement was repeated at least three times.

Supporting Information

Supporting Information is available from the Wiley Online Library or from the author.

Acknowledgements

This study was financially supported by the National Key Research and Development Program (Grant No. 2018YFA0703102) and the National Natural Science Foundation (Grant No. 51733006).

Conflict of Interest

The authors declare no conflict of interest.

Keywords

adhesive, chain extender, hydrogen bonding, polyurethane elastomer, self-healing

Received: August 17, 2020
Revised: September 17, 2020
Published online:

- [1] a) P. Krol, *Prog. Mater. Sci.* **2007**, *52*, 915; b) E. Delebecq, J. P. Pascault, B. Boutevin, F. Ganachaud, *Chem. Rev.* **2013**, *113*, 80.
- [2] a) T. Gurunathan, C. R. K. Rao, R. Narayan, K. V. S. N. Raju, *J. Mater. Sci.* **2013**, *48*, 67; b) V. García-Pacios, V. Costa, M. Colera, J. M. Martín-Martínez, *Prog. Org. Coat.* **2011**, *71*, 136; c) M. L. Pinto, S. Dias, J. Pires, *ACS Appl. Mater. Interfaces* **2013**, *5*, 2360; d) A. Levitt, S. Seyedin, J. Zhang, X. Wang, J. M. Razal, G. Dion, Y. Gogotsi, *Small* **2020**, *16*, 2002158.
- [3] a) D. Wang, J. Xu, J. Chen, P. Hu, Y. Wang, W. Jiang, J. Fu, *Adv. Funct. Mater.* **2019**, *30*, 1907109; b) Y. Lin, G. Li, *J. Mater. Chem. B* **2014**, *2*, 6878.
- [4] a) C. Jin, G. Sinawang, M. Osaki, Y. Zheng, H. Yamaguchi, A. Harada, Y. Takashima, *Polymers* **2020**, *12*, 1393; b) L. Xiao, J. Shi, K. Wu, M. Lu, *React. Funct. Polym.* **2020**, *148*, 104482.
- [5] a) Z. Wang, C. Xie, C. Yu, G. Fei, Z. Wang, H. Xia, *Macromol. Rapid Commun.* **2018**, *39*, 1700678; b) Y. Li, W. Guo, W. Li, X. Liu, H. Zhu, J. Zhang, X. Liu, L. Wei, A. Sun, *Chem. Eng. J.* **2020**, *393*, 124583.
- [6] a) N. Duan, Z. Sun, Y. Ren, Z. Liu, L. Liu, F. Yan, *Polym. Chem.* **2020**, *11*, 867; b) S. Chen, F. Mo, Y. Yang, F. J. Stadler, S. Chen, H. Yang, Z. Ge, *J. Mater. Chem. A* **2015**, *3*, 2924.
- [7] a) S. Burattini, B. Greenland, D. Merino, W. Weng, J. Seppala, H. Colquhoun, W. Hayes, M. Mackay, I. Hamley, S. Rowan, *J. Am. Chem. Soc.* **2010**, *132*, 12051; b) A. Feula, A. Pethybridge, I. Giannakopoulos, X. Tang, A. Chippindale, C. R. Siviour, C. P. Buckley, I. W. Hamley, W. Hayes, *Macromolecules* **2015**, *48*, 6132.
- [8] a) S. M. Kim, H. Jeon, S. Shin, S. Park, J. Jegal, S. Hwang, D. Oh, J. Park, *Adv. Mater.* **2018**, *30*, 1705145; b) A. Rekondo, R. Martin, A. Luzuriaga, G. Cabanero, H. Grande, I. Odriozola, *Mater. Horiz.* **2014**, *1*, 237.
- [9] a) S. Söntjens, R. Renken, G. Gemert, T. Engels, A. Bosman, H. Janssen, L. Govaert, F. Baaijens, *Macromolecules* **2008**, *41*, 5703; b) S. Chen, N. Mahmood, M. Beiner, W. H. Binder, *Angew. Chem., Int. Ed. Engl.* **2015**, *54*, 10188; c) J. Xu, S. Ye, C. Ding, L. Tan, J. Fu, *J. Mater. Chem. A* **2018**, *6*, 5887.
- [10] Y. Yang, Z. Ye, X. Liu, J. Su, *J. Mater. Chem. C* **2020**, *8*, 5280.
- [11] X. Wu, J. Wang, J. Huang, S. Yang, *ACS Appl. Mater. Interfaces* **2019**, *11*, 7387.
- [12] Y. Chen, A. M. Kushner, G. A. Williams, Z. Guan, *Nat. Chem.* **2012**, *4*, 467.
- [13] J. Hentschel, A. Kushner, J. Ziller, Z. Guan, *Angew. Chem., Int. Ed.* **2012**, *51*, 10561.
- [14] a) M. Khatib, O. Zohar, W. Saliba, S. Srebnik, H. Haick, *Adv. Funct. Mater.* **2020**, *30*, 1910196; b) H. Guo, Y. Han, W. Zhao, J. Yang, L. Zhang, *Nat. Commun.* **2020**, *11*, 2037; c) Y. Lai, X. Kuang, P. Zhu, M. Huang, X. Dong, D. Wang, *Adv. Mater.* **2018**, *30*, 1802556.
- [15] a) Y. Song, Y. Liu, T. Qi, G. L. Li, *Angew. Chem., Int. Ed. Engl.* **2018**, *57*, 13838; b) W. Wang, H. Chen, Q. Dai, D. Zhao, Y. Zhou, L. Wang, D. Zeng, *Smart Mater. Struct.* **2019**, *28*, 015008; c) W. Fan, Y. Jin, L. Shi, R. Zhou, W. Du, *J. Mater. Chem. A* **2020**, *8*, 6757.
- [16] a) Z. Liu, L. Zhang, Q. Guan, Y. Guo, J. Lou, D. Lei, S. Wang, S. Chen, L. Sun, H. Xuan, E. M. Jeffries, C. He, F. L. Qing, Z. You, *Adv. Funct. Mater.* **2019**, *29*, 1901058; b) L. Zhang, Z. Liu, X. Wu, Q. Guan, S. Chen, L. Sun, Y. Guo, S. Wang, J. Song, E. M. Jeffries, C. He, F. L. Qing, X. Bao, Z. You, *Adv. Mater.* **2019**, *31*, 1901402; c) C. H. Li, C. Wang, C. Keplinger, J. L. Zuo, L. Jin, Y. Sun, P. Zheng, Y. Cao, F. Lissel, C. Linder, X. Z. You, Z. Bao, *Nat. Chem.* **2016**, *8*, 618.
- [17] a) X. Dai, Y. Zhang, L. Gao, T. Bai, W. Wang, Y. Cui, W. Liu, *Adv. Mater.* **2015**, *27*, 3566; b) Y. Wu, H. Wang, F. Gao, Z. Xu, F. Dai, W. Liu, *Adv. Funct. Mater.* **2018**, *28*, 1801000; c) H. Wang, Y. Wu, C. Cui, J. Yang, W. Liu, *Adv. Sci.* **2018**, *5*, 1800711; d) F. Gao, C. Ruan, W. Liu, *Mater. Chem. Front.* **2019**, *3*, 1736; e) Z. Xu, W. Liu, *Chem. Commun.* **2018**, *54*, 10540.
- [18] F. Xie, T. Zhang, P. Bryant, V. Kurusingal, J. M. Colwell, B. Laycock, *Prog. Polym. Sci.* **2019**, *90*, 211.
- [19] a) D. Tian, F. Wang, Z. Yang, X. Niu, Q. Wu, P. Sun, *Carbohydr. Polym.* **2019**, *219*, 191; b) J. Liu, D. J. Martin, R. J. Moon, J. P. Youngblood, *J. Appl. Polym. Sci.* **2015**, *132*, 41970.
- [20] J. Kang, D. Son, G. N. Wang, Y. Liu, J. Lopez, Y. Kim, J. Y. Oh, T. Katsumata, J. Mun, Y. Lee, L. Jin, J. B. Tok, Z. Bao, *Adv. Mater.* **2018**, *30*, 1706846.
- [21] a) T. Li, A. J. Senesi, B. Lee, *Chem. Rev.* **2016**, *116*, 11128; b) Y. Zhang, H. Gao, H. Wang, Z. Xu, X. Chen, B. Liu, Y. Shi, Y. Lu, L. Wen, Y. Li, Z. Li, Y. Men, X. Feng, W. Liu, *Adv. Funct. Mater.* **2018**, *28*, 1705962.
- [22] J. Y. Chung, M. K. Chaudhury, *J. Adhes.* **2005**, *81*, 1119.
- [23] a) B. T. Michal, E. J. Spencer, S. J. Rowan, *ACS Appl. Mater. Interfaces* **2016**, *8*, 11041; b) S. Wang, Z. Liu, L. Zhang, Y. Guo, J. Song, J. Lou, Q. Guan, C. He, Z. You, *Mater. Chem. Front.* **2019**, *3*, 1833.
- [24] W. Li, L. Bouzidi, S. Narine, *Ind. Eng. Chem. Res.* **2008**, *47*, 7524.
- [25] a) M. Sun, C. Y. Hong, C. Y. Pan, *J. Am. Chem. Soc.* **2012**, *134*, 20581; b) W. Lee, Y. Bae, A. J. Bard, *J. Am. Chem. Soc.* **2004**, *126*, 8358.
- [26] a) B. Liu, H. Zhang, S. Liu, J. Sun, X. Zhang, B. Z. Tang, *Mater. Horiz.* **2020**, *7*, 987; b) L. Song, T. Zhu, L. Yuan, J. Zhou, Y. Zhang, Z. Wang, C. Tang, *Nat. Commun.* **2019**, *10*, 1315.
- [27] Y. Huang, J. Xing, Q. Gong, L. C. Chen, G. Liu, C. Yao, Z. Wang, H. L. Zhang, Z. Chen, Q. Zhang, *Nat. Commun.* **2019**, *10*, 169.
- [28] a) J. Luo, Z. Xie, J. W. Lam, L. Cheng, H. Chen, C. Qiu, H. S. Kwok, X. Zhan, Y. Liu, D. Zhu, B. Z. Tang, *Chem. Commun.* **2001**, *18*, 1740; b) J. Li, J. Wang, H. Li, N. Song, D. Wang, B. Z. Tang, *Chem. Soc. Rev.* **2020**, *49*, 1144.
- [29] a) Y. Chen, R. P. Sijbesma, *Macromolecules* **2014**, *47*, 3797; b) J. Tan, R. Zou, J. Zhang, W. Li, L. Zhang, D. Yue, *Nanoscale* **2016**, *8*, 4742; c) T. Wang, X. Zhang, Y. Deng, W. Sun, Q. Wang, F. Xu, X. Huang, *Polymers* **2017**, *9*, 411.
- [30] L. Bergamonti, C. Graiff, M. Tegoni, G. Predieri, L. Bellot-Gurlet, P. P. Lottici, *Spectrochim. Acta, Part A* **2017**, *171*, 515.